Chapter

Germanium on Silicon Avalanche Photodiode for High-Speed fiber Communication

Mengyuan Huang, Kelly Magruder, Yann Malinge, Parastou Fakhimi, Hao-Hsiang Liao, David Kohen, Gregory Lovell, Wei Qian, Kiyoung Lee, Carsten Brandt, Mahtab Hakami, Yen-jung Chen, Erin Carabajal, Erle Guillermo, Seth Slavin and Ansheng Liu

Abstract

Silicon photonics is one of the promising technologies for high-speed optical fiber communications. Among various silicon photonic devices, germanium on silicon avalanche photodiode (Ge/Si APDs) received tremendous attentions because of its superior performance and integration compatibility. In 2016, normal incidence Ge/Si APD demonstrated a NRZ 10^{-12} sensitivity of −23.5 dBm at 25 Gb/s; more recently, a waveguide-integrated Ge/Si APD receiver presents a 106Gb/s PAM4 sensitivity of −18.9 dBm. These results are best reported performance among all APD-based devices, and these breakthroughs are mainly benefited from Ge/Si APD's structure and material characteristics. Ge/Si APD adopts a separated charge-absorption-multiplication (SCAM) structure with a pure Ge absorber and an intrinsic Si avalanche layer. Since, Si is one of well-known best avalanche materials with large gain-bandwidth products and low ionization noise ratio, which make Ge/Si APDs demonstrating superior performance at high data rates. Moreover, this Si-based device is manufactured by standard CMOS foundries and is process-compatible with other silicon photonic devices including silicon-based waveguides, demux, hybrid, etc. This advantage simplifies the assembly of photonic systems and makes a large-scale integrated silicon photonic chip possible, which provides compact solutions for high-density communication systems. In this chapter, we review recent progresses on Ge/Si APD structure design, material, and performance.

Keywords: silicon photonics, avalanche photodiode, high-speed, germanium on silicon, Fiber communication

1. Introduction

Data traffic grows exponentially in last few years [1–4]. From 2018 to now, the global digital data creation experiences a compound annual growth rate of 25% [5], and the estimated annual data traffic will be four times larger at 2025 [6]. All these fast-expending data demands are accommodated by fiber communication systems. In nowadays, more than 20% interconnects in data centers already reach operating data rate of 100 Gb/s per lane [7]. To maximize bandwidth efficiency, latest systems adopt various technologies including wavelength division-multiplexing (WDM), complex modulations (PAM4), etc., which are inevitable to bring more penalties from original ones. For instance, CWDM technology typically causes ~4.5 dB loss on optical powers [8] and complex PAM4 modulation brings 4.8 dB loss compared to simple NRZ modulation [9, 10]. Therefore, a high-speed and high-sensitivity solution is essential to compensate these extra losses and to support the upgrades of data and telecommunication systems to new generation.

Avalanche photodiode (APD) and coherent detection are most promising solutions with gains. Compared to coherent detection, APD receivers have a variety of advantages including smaller size, lower power consumptions, better latency, and lower cost [11]. These merits make the large-scale deployment of APDs into high-sensitivity systems. One example is the 29 dB-link budget requirement in 10 Gb/s passive optical networks (PON) [12]. Photodiodes (PD) cannot meet such high requirement, and APDs provide extra ~8 dB gains at data rate of 10 Gb/s or 25 Gb/s [13–15]. Thus, millions of APD devices are utilized in PON systems for fiber-to-home applications. However, when bandwidth is increased to 100 Gb/s in today, traditional APD's additional gain drops to 2–4 dB [16, 17] that is related to InP-based material fundamental limitations (poor gain-bandwidth products) [18]. On the other hand, Ge/Si APD demonstrated a great linear gain-bandwidth products of 340 GHz [19], which are the fundamental reasons of Ge/Si APD presenting better performance at higher data rates such as 100 Gb/s and beyond.

2. Ge/Si APD structure and responsivity improvement

The first demonstration of high-speed Ge/Si APD was completed by Intel in 2007 [20], and that device shows a 3 dB bandwidth of 7 GHz at gain = 1. This device is a top-illuminated device on bulk Si wafer, and device's main functional layers include a heavily n-doped silicon contact layer, a 0.5 μm thick intrinsic silicon multiplication layer, a 0.1 μm thick p-type silicon charge layer, a 1 μm thick pure germanium absorption layer, and a 0.1 μm heavily p-doped germanium contact layer as shown in **Figure 1**.

This APD reports a responsivity of 0.52 A/W at 1310 nm, which is obvious worse than 10 Gb/s III-V APD's responsivity of 0.85 A/W [21]. The fundamental reason is that Ge's absorption coefficients are worse than $In_{0.53}Ga_{0.47}As$ at O-band wavelengths. To improve Ge/Si device's responsivity, there have two promising designs including resonant cavity-enhanced (RCE) structure and waveguide-integrated structure.

2.1 RCE normal incidence Ge/Si avalanche photodiode

RCE photodiode structure is studied by several groups using various materials [22, 23]. The principle is adding both top and bottom reflectors to photodiodes' active layers for forming a Fabry-Perot resonant cavity. The RCE design provides a multi-pass absorption scheme for responsivity improvement but no impact on high-speed characteristics. RCE photodiode's quantum efficiency is given by following formula [23]:

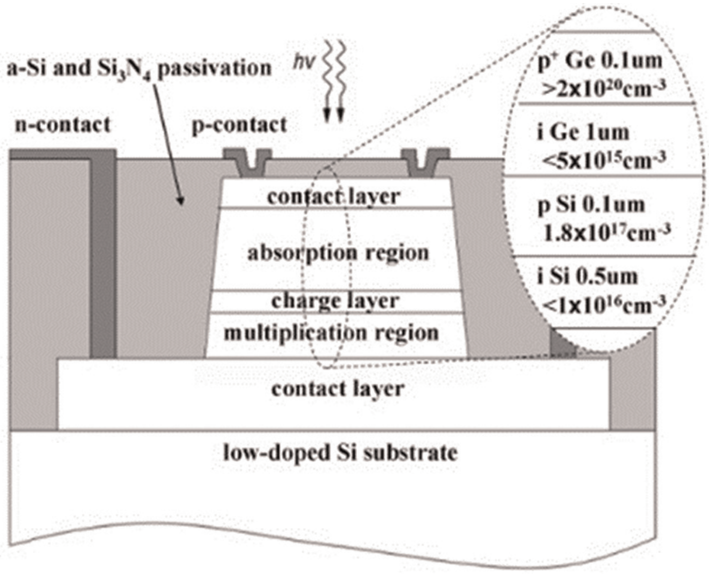

Figure 1.
Cross section of Ge/Si APD on bulk Si substrate [20].

$$\eta_{RCE} = \left(\frac{1 + R_2 \exp(-\alpha d)}{1 - 2\sqrt{R_1 R_2} \exp(-\alpha d) \cos(2\beta L) + R_1 R_2 \exp(-\alpha d)} \right) (1 - R_1)(1 - \exp(-\alpha d)) \quad (1)$$

Here, R_1 is the reflectivity at top surface of RCE cavity, and R_2 is the reflectivity at bottom surface, α is absorption coefficient, d is absorber thickness, L is the cavity length, and β is the propagation constant.

Considering photodiode's top surface is typically made by antireflection (AR) coating with low reflectivity <5%, a high reflectivity surface at bottom is critical for enhancing responsivity. Several papers reported Ge/Si RCE devices by using different bottom reflectors [24–27]. One common solution is using SOI substrate: a reflection happens at the interface between Si and buried oxide (BOX) layers because of large refractive index gap. Especially for double SOI substrate, the bottom reflectivity can reach >90% with optimized silicon and oxide thicknesses [24]. Alternative method is to use CMOS-compatible metals such as aluminum with >95% reflectivity at optical communication wavelengths (**Figure 2**) [28].

Figure 3 presented measured 25 Gb/s NIAPDs' responsivity with and without RCE structure. We can clearly see that: after achieving a > 100% improvement on responsivity at peak wavelengths (1310–1314 nm), the RCE device's optical bandwidth becomes narrower like full width at half maximum ~40 nm.

Resonated photodiode's optical bandwidth is related by free spectral range (FSR) and Finesse (F), the full width at half maximum (FWHM) is given by following equation [29]:

$$FWHM = \frac{FSR}{F} = \frac{\lambda^2}{2n_{eff}L} \times \frac{1 - \sqrt{R_1 R_2} e^{-\alpha d}}{\pi (R_1 R_2)^{1/4} e^{-\frac{\alpha d}{2}}} \quad (2)$$

Here, λ is operating wavelength, n_{eff} is the effective refractive index, and L is the total length of RCE cavity. Since, Ge/Si photodetector has thin absorption layer (e.g.

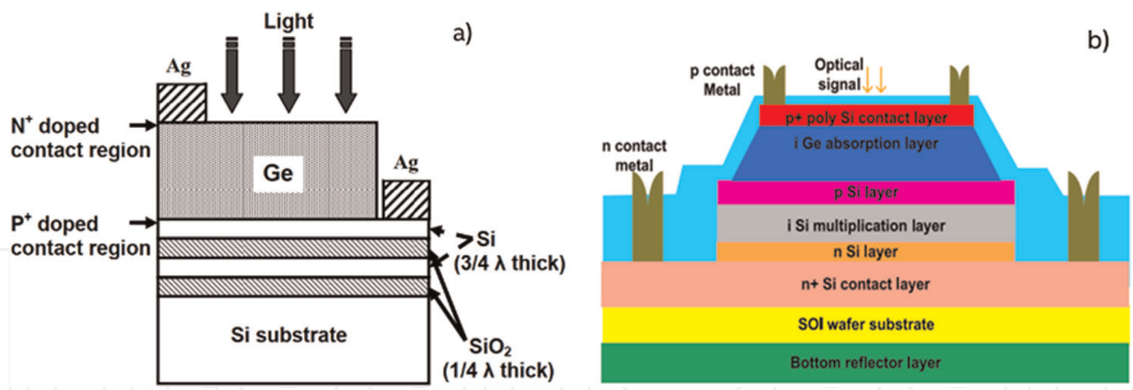

Figure 2.
a) Ge/Si PD on DSOI [24]; b) Ge/Si APD with metal reflector [27].

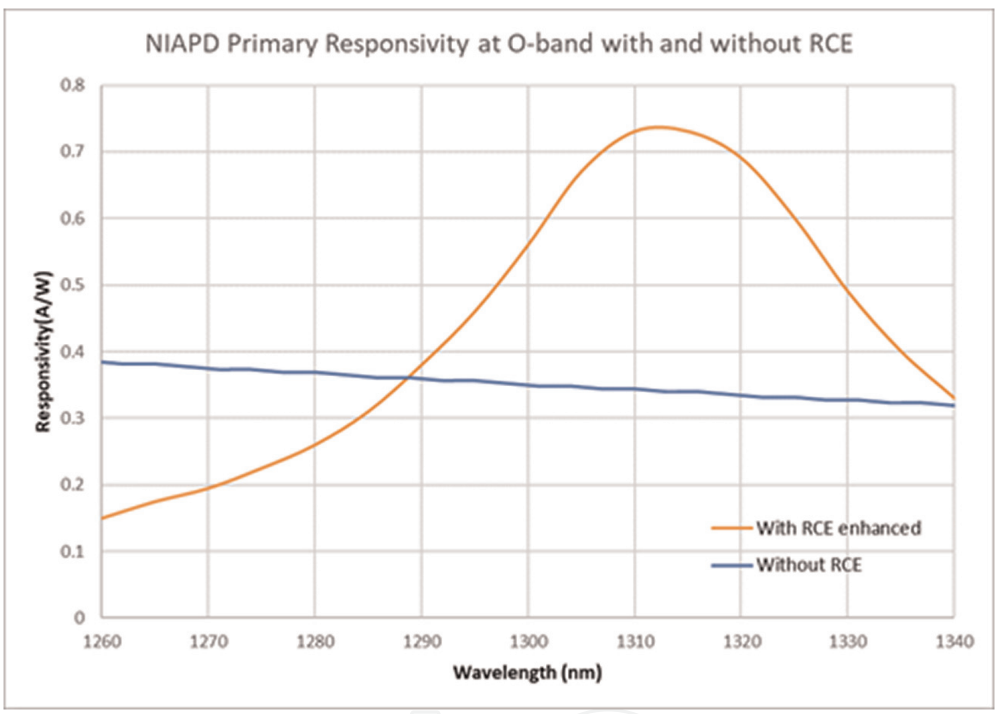

Figure 3.
NIAPD responsivity with and without RCE at CWDM4 wavelengths.

<600 nm) for high-speed operations, which brings a narrow optical 3 dB bandwidth (e.g. <50 nm) and not suitable for current 2–10 km data centers systems using multiples wavelengths like CWDM4 [30, 31].

2.2 Waveguide-integrated Ge/Si avalanche photodiode

Waveguide structure has better solutions with high bandwidth and flat optical spectrum simultaneously. The fundamental improvement of waveguide photodiode is that photon-generated carriers move into a different direction from optical propagations, which breaks the trade-off between 3 dB bandwidth and responsivity on normal incident devices.

Figure 4 presents evanescent coupling Ge/Si WGAPD devices [32]. In this design, on-chip optical power is confined by Si waveguide and propagates to WGAPD. Ge/Si WGAPD's critical layers—Si multiplication, charge, and Ge absorption layers—are

DOI: http://dx.doi.org/10.5772/intechopen.107971

grown on these Si waveguide layers. Therefore, it has an unavoidable height between silicon waveguide and Ge absorber, which degrades coupling efficiency and responsivity [33]. For instance, evanescent Ge/Si WGAPD only shows 0.6 A/W responsivity at 1550 nm even with 50 μm length Ge absorber [34].

Optimized waveguide design is recently reported recess-type structure [2], which solves height difference by etching a recess into Si waveguide and selectively depositing Si and Ge films into the recess. Therefore, the gap between Si waveguide and Ge absorber is minimized; as a result, evanescent device's responsivity is improved >0.75 A/W [2]. **Figure 5** presents the schematic cross section of recess-type Ge/Si waveguide APD.

Another advantage of this recess structure is using thick top Si waveguide, which supports both TE and TM modes with low propagation losses. This structure only needs one-side input optical waveguide without polarization rotator-splitter, which reduces optical losses and improves external responsivity and overall performance.

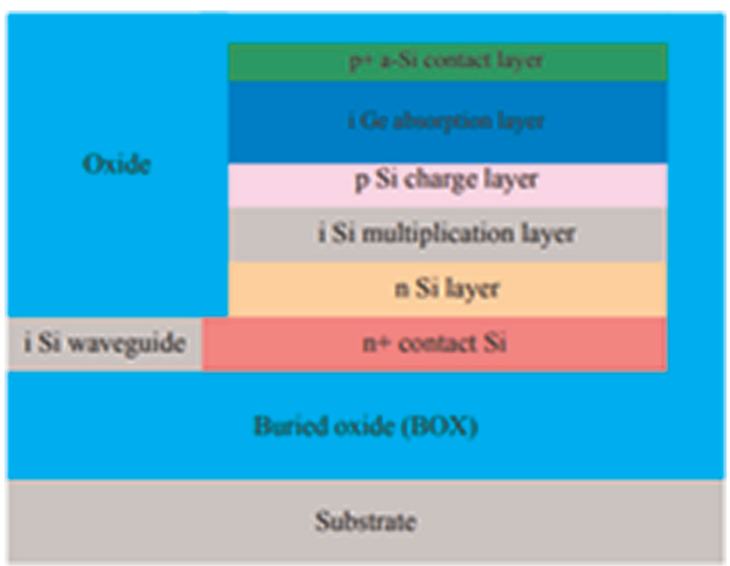

Figure 4.
Waveguide-integrated Ge/Si APD using evanescent coupling [32].

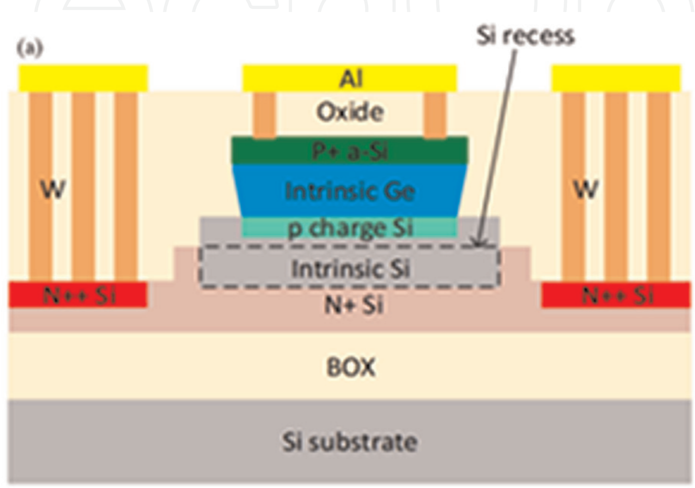

Figure 5.
Recess-type waveguide-integrated Ge/Si avalanche photodiode [2].

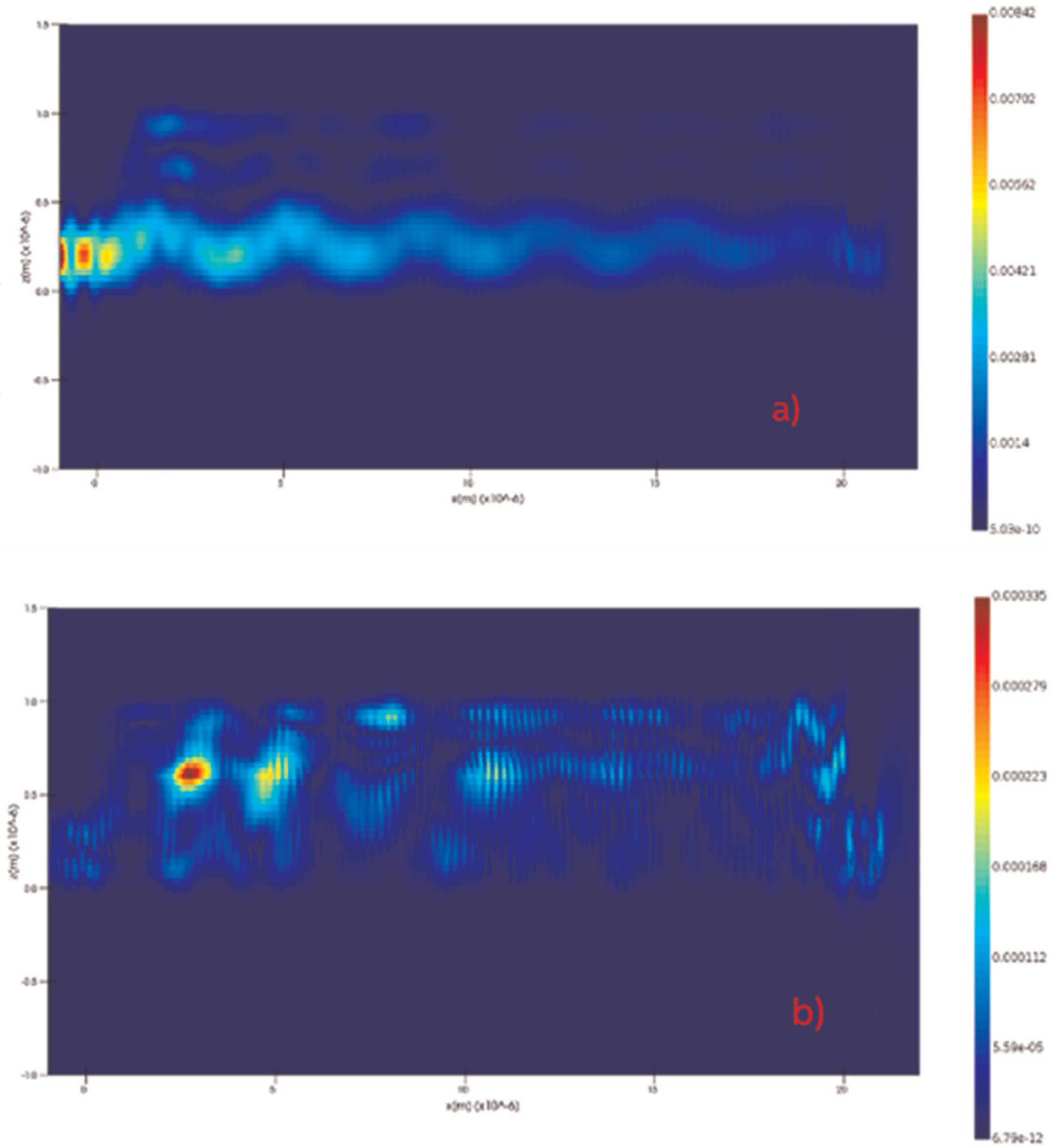

Figure 6.
a) TE mode and b) TM mode propagation in recess-type Ge/Si WGAPD.

Figure 6 shows technology computer-aided design (TCAD) simulations of both TE and TM modes propagations in this recess-type WGAPD structure:

Figure 7 presents measured primary responsivity (gain = 1) of recess-type Ge/Si APD. This result is extracted by WGPD structure using similar film thickness as WGAPD, which shows a flat responsivity from 1260 to 1340 nm wavelengths and suitable for CWDM4 system applications.

3. Ge/Si interface and Ge/Si APD RF performance

Ge/Si devices' RF performance is discussed by several groups [35, 36]. However, several critical effects were not comprehensively studied. For instance, Ge/Si interface characteristics play an important role on APDs' RF performance, because all photon generated electrons must across this interface for electrical amplifications. Because of 4.2% lattice mismatch between Ge and Si substrate, a variety of dislocations are

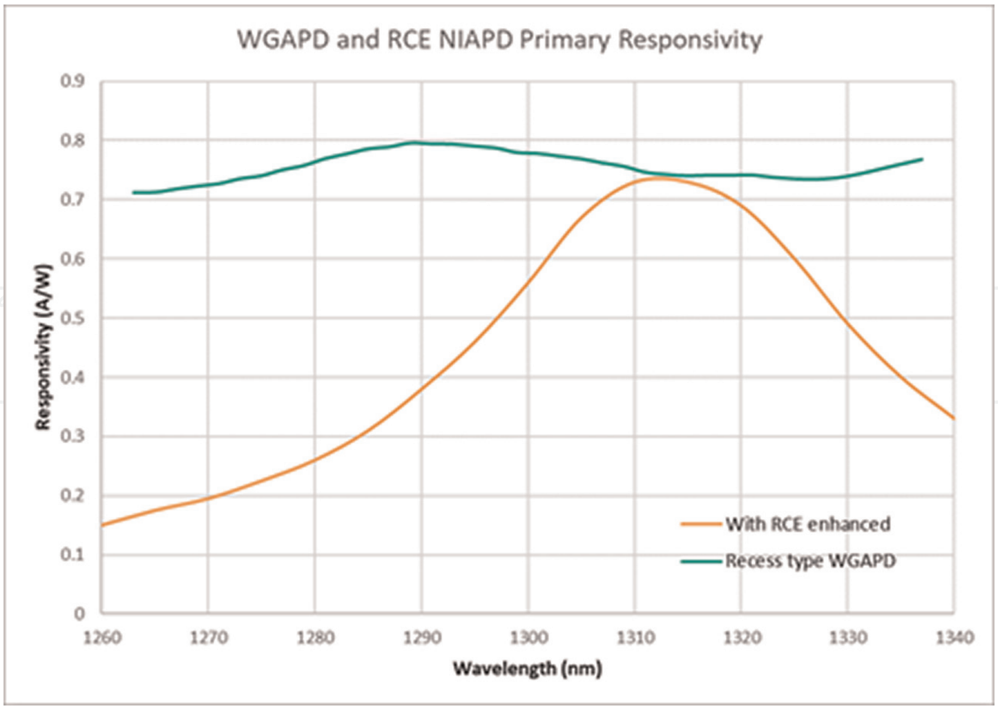

Figure 7.
WGAPD and NIAPD primary responsivity at CWDM4 wavelengths.

formed inside Ge epitaxial layer. Especially at Ge/Si interface, threading dislocation density typically reaches $1\times10^{10}/cm^2$ [37]; in additional, volumes of misfit dislocations [38] and lots of unpaired dangling bonds [39] locate at the interface region. These characteristics cause several undesirable impacts on APDs' RF performance.

3.1 Shallow-level defect states and its impact on RF performance

For Ge on Si films, different groups reported the observations of dislocations-related deep-level defect states with energy level of 0.37 eV [40, 41]. This defect state captures free electrons for non-radiative recombination and contributes to devices' dark currents [42].

Different from deep-level defect states, shallow defect level state also found inside Ge on Si film, which has an energy level of 0.02 eV above valence band and behaviors as acceptors [43]. The fundamental formation of this shallow-level defect state could be explained by unpaired dangling bonds at Ge/Si interface. Since Si lattice constant (5.431 Å) is smaller than Ge (5.658 Å), many Si atoms ($\sim10^{13}$ atoms/cm^2) are unpaired at Ge/Si interface, which attract electrons like p-type dopants for forming a stable covalence bond (**Figure 8**).

Several groups reported the existence of this shallow-level defect states by using various Ge growth methods including ultra-high vacuum chemical vapor deposition (UHV-CVD), reduced pressure chemical vapor deposition (RPCVD), and sputter [43–45]. **Figure 9** provides a summary of shallow-level defect state's effective concentration. Based on reported data, defect effective carrier concentrations are increasing near Ge/Si interface region. This phenomenon has similar trend of material data: there have more unpaired bonds and more dislocations close to Ge/Si interface.

This shallow-level defect state brings serious impacts on device's electrical performance. First, high concentration reduces the mobility of photon-generated carriers. For example, although hole mobility reaches 1900 cm^{2}V^{-1} in intrinsic Ge film [46],

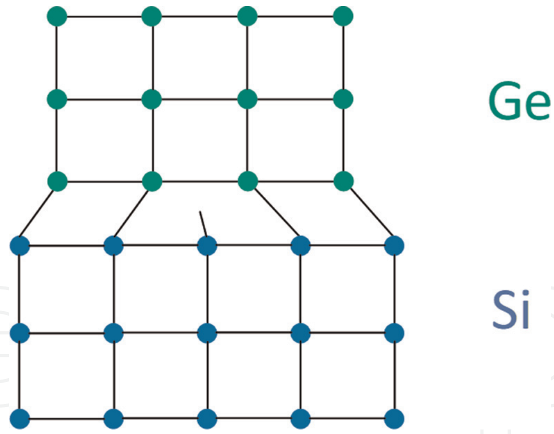

Figure 8.
Ge/Si interface atom distribution and dangling bonds.

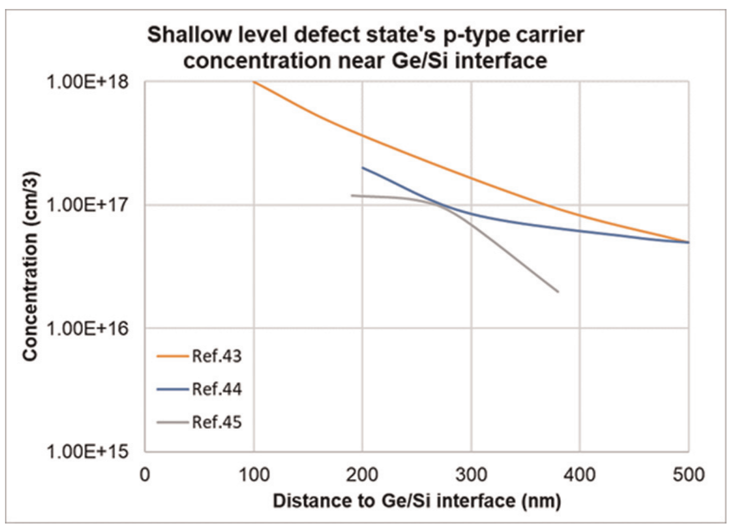

Figure 9.
Shallow-level defect states' concentration at Ge/Si interface ref. [43–45].

the number drops to only ~45 cm^2V^{-1} [43] at defect carrier concentration of 2×10^{17} cm^{-3}. Such mobility degradation significantly increases diffusion time in Ge and then reduces 3 dB bandwidth.

Based on reported data, a 250–350 nm thick Ge with concentration > $10^{17}/cm^3$ is found close to Ge/S interface. This p-type doped region requires high bias for depletion and for carrier reaching saturation velocity. **Figure 10a)** and **b)** present the E-field distribution comparison with and without shallow-level defect state:

Figure 10c) presents local electrical field intensity dependence on defect states' carrier concentrations. Given a 250 nm-thick Ge layer with 1×10^{17} cm^{-3} concentration, the local E-field reaches ~150 kV/cm which can easily charge carriers energy beyond avalanche threshold inside Ge [47, 48]. Considering poor Ge's ionization coefficient ratio, e. g. ~1 [49], APD device's transit time bandwidth is significantly degraded with avalanching in Ge layer [50]. If this defect effective concentration is even larger like >2×10^{17} cm^{-3}, the depleted region will have an E-field >200 kV/cm with even worse impacts like huge leakage currents from band-to-band tunneling effects [51]. These problems completely ruin high-speed APD devices. Therefore, it is extremely critical to control of Ge/Si interface quality and many methods—like dilute HF-last pre-clean, high-temp pre-bake, low-temp pre-bake with HCl clean, in situ process—had been studied [52–55].

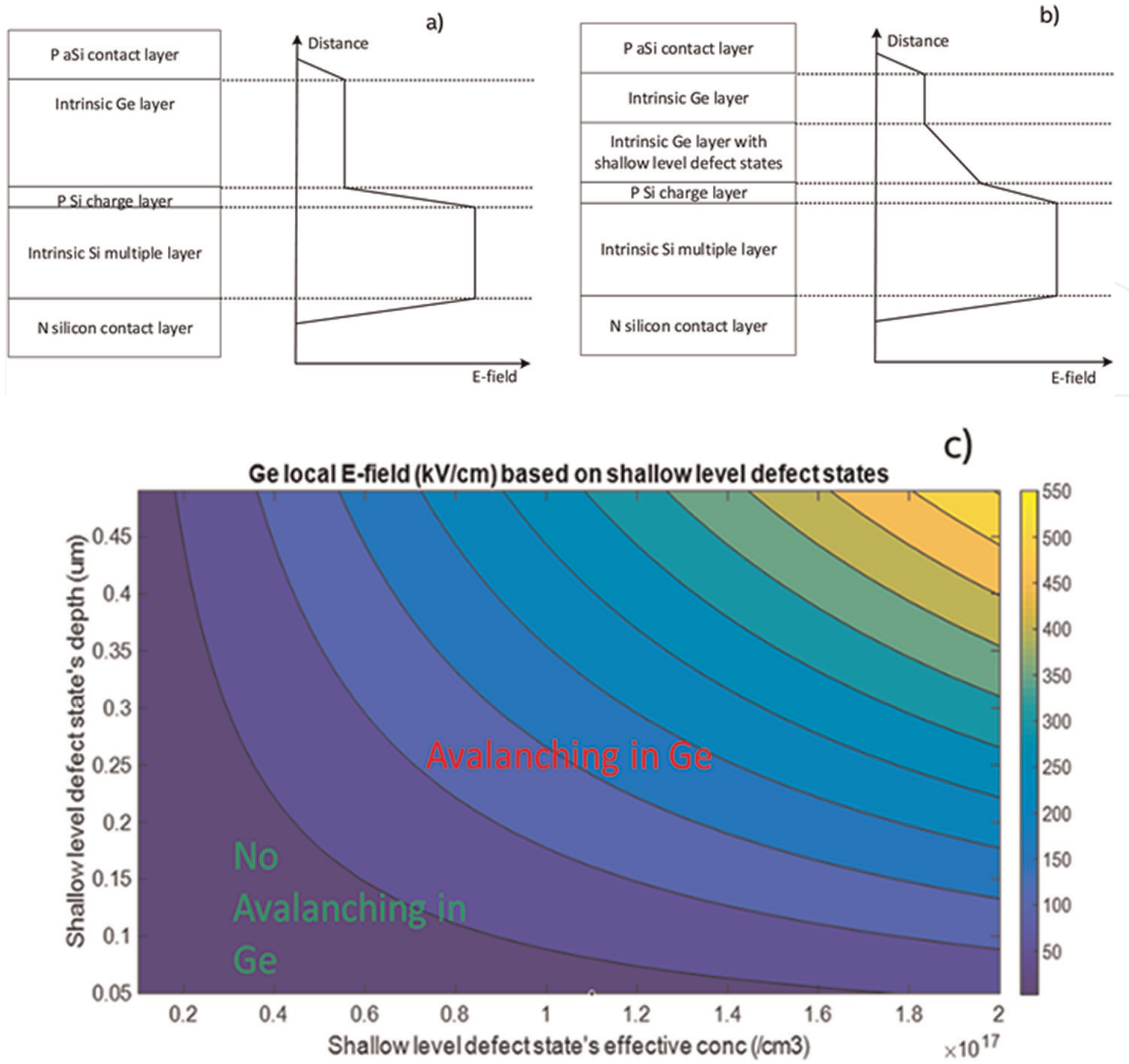

Figure 10.
a) Ge/Si APD's ideal E-field; b) Ge/Si APD's E-field with shallow-level defect states at Ge/Si interface; c) E-field need to deplete shallow-level defect states.

3.2 Ge/Si heterojunction and impact on RF performance

Ge/Si heterojunction is important for understanding carrier transport mechanisms inside APD devices. Because Ge has an electron affinity of 4.0 eV close to Si value of 4.05 eV, different types of Ge/Si band alignment had been reported. Several studies show Ge/Si type-I heterojunction [56–58], and other papers reported type-II heterojunction [59–61]. To better understand this issue, we investigated free carrier distributions at Ge/Si interface by using two different silicon substrates (either heavily p-doped or heavily n-doped) (**Figure 11**).

Based on measured data, samples on either N-substrate or P-substrate show carriers' accumulations at Ge/Si interface, which proves type-I heterojunctions because type-II band offset has no barrier for electrons' accumulations.

Device-level data also support type-I heterojunction. **Figure 12** shows measured WGAPD S21 curves under different biases. At operating with bias lower than breakdown voltage (V_{br}), APD's S21 response is decreasing at high frequency with a 3 dB bandwidth of 27.5 GHz. While, at high bias beyond breakdown voltage, RF enhancement and peaking happen on APD's S21 curves and then 3 dB bandwidths are

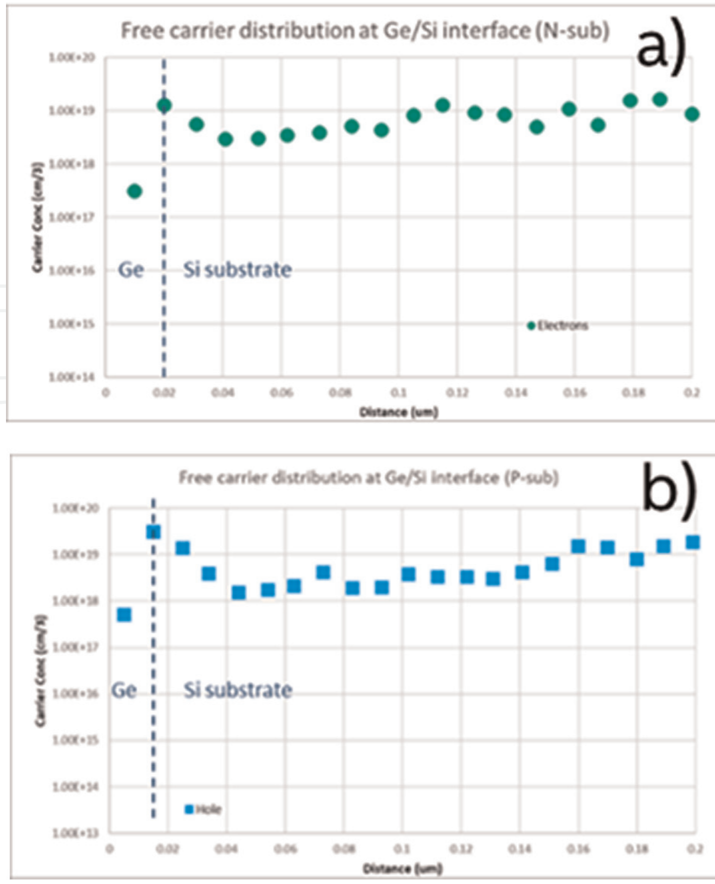

Figure 11.
Measured free carrier distribution at Ge/Si interface: a) N-sub and b) P-sub.

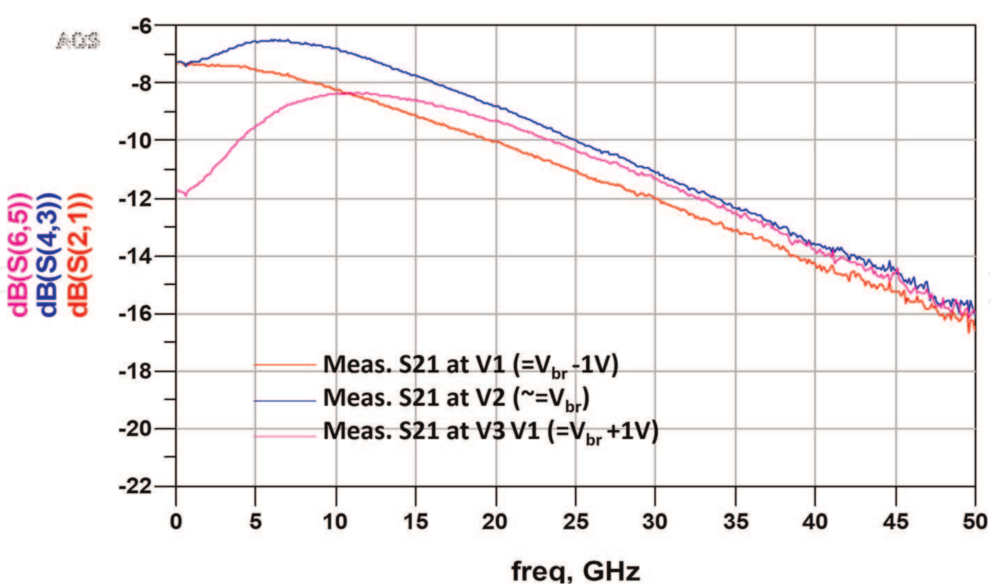

Figure 12.
Measured S21 curves of Ge/Si APD under different bias.

increased significantly. These frequency response peaking and bandwidth enhancements are related to negative differential resistance (NDR) effect [62, 63].

NDR effect has been frequently observed in quantum wells photonic devices, and tunneling effect is used to explain this phenomenon [64, 65]. However, Ge/Si APD utilizes bulk Ge on Si without quantum well; thus, the only possible energy barrier is the conduction band offset from type-I Ge/Si heterojunction. Another evidence is that NDR enhanced 3 dB bandwidths only happened at Ge/Si APD with bias ranges beyond V_{br} causing a local high E-field, which is significantly increasing the possibility of electrons' tunneling at Ge/Si interface as following diagram (**Figure 13**):

3.3 Re-visit Ge/Si APD's gain-bandwidth product

Because of the NDR effect existence, it is necessary to revisit Ge/Si APDs' reported gain-bandwidth products. **Table 1** summarized published Ge/Si APD gain-bandwidth data with and without NDR effect.

Based on reported data, the same APD device's shows obviously larger gain-bandwidth product under NDR effect. However, such high-performance region is not suitable for high-speed communication applications. One reason is that APDs' S21 responses have frequencies-related peaking and drops, which bring drawbacks including variations in group delay [72] and receiver's DC responsivity losses. Another reason is that NDR effect only happens at bias $>V_{br}$, which led to high dark currents (e.g. >1 mA) and high shot noise. Moreover, mA-level dark currents cannot meet several commercial transceivers' requirements such as loss of signals (LOS) under weak input optical powers [73]. In summary, APD under NDR is not suitable for high-speed communication systems, but it can be applied to single-photon detection like Geiger-mode operations [74].

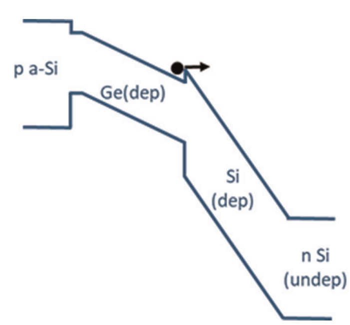

Figure 13.
Ge/Si APD band structure under high E-field and NDR effect.

Operating type	Gain-bandwidth product (without NDR)	Gain-bandwidth product (with NDR)	Ref
Ge/Si NIAPD	340 GHz	—	[16]
	—	840 GHz	[66]
	258 GHz	—	[67]
	300 GHz	450 GHz	[68]
Ge/Si WGAPD	360 GHz	—	[69]
	—	310 GHz	[70]
	280 GHz	410 GHz	[71]
	300 GHz	—	[2]
Applications	High-speed communication	Single photo detection	

Table 1.
Reported Ge/Si APD w/ and w/o NDR effect.

3.4 Ge/Si APD equivalent circuit model

High-speed photodiodes' or APD's equivalent circuit model had been investigated by different groups [70, 71, 75]. Typically, the circuit model includes transit time and RC-time circuit models. The RC-time model in equivalent circuit contains both APD junction parameters and parasitic parameters, which can be extracted by using fitting results of S22 as shown in **Figure 14(b)**. Different from III-V APDs on semi-insulating substrate, Ge/Si APD device is developed on a SOI wafer with a thick buried oxide layer (1-3 μm) with a great RF isolation. Thus, parasitic components have weak impact on Ge/Si APD's RF characteristics, and **Table 2** presents values extracted by circuit model.

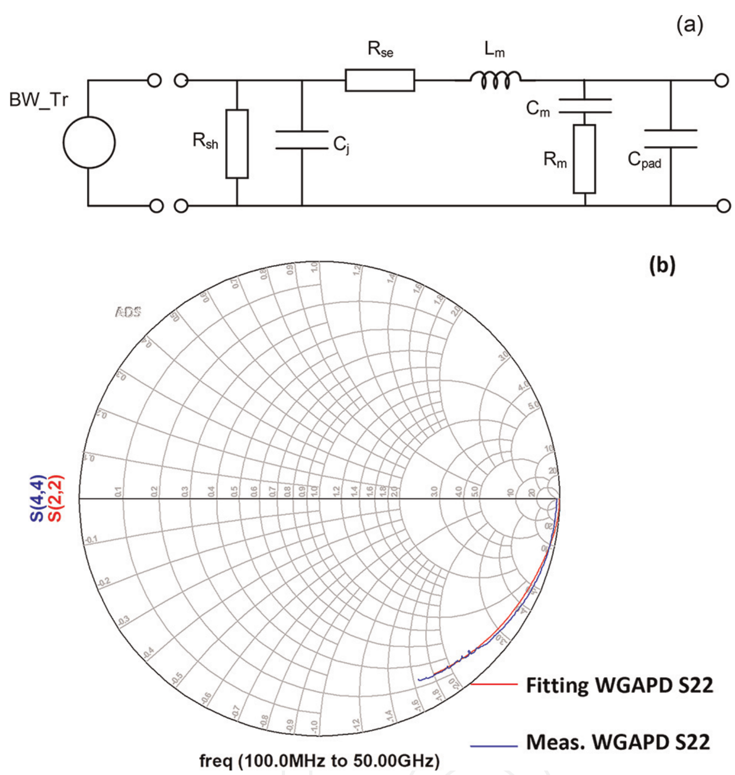

Figure 14.
a) Ge/Si APD circuit model; b) Ge/Si APD S22 measured and fitting results.

Parameter	Symbol	Value
Shunt resistance	R_{sh}	4.6 MΩ
Junction capacitance	C_j	22.4 fF
Series resistance	R_{se}	13.4 Ω
Metal inductance	L_m	140 pH
Pad capacitance	C_{pad}	5.5 fF
Metal/sub-capacitance	C_m	6.4 fF
Metal/sub-resistance	R_m	1.6 kΩ

Table 2.
106 Gb/s Ge/Si WGAPD junction and parasitic parameters.

4. Ge/Si APD receiver performance and applications

4.1 Ge/Si APD receiver's RF model

The RF model of entire Ge/Si APD receiver is the combination of APD equivalent circuit model, transimpedance amplifier (TIA) model, interconnect model, and evaluation board's model shown as **Figure 15(a)**. The interconnect between APD and TIA is generally achieved by a short gold wire, which typically can be considered a small inductor [76]. With proper modeling of receiver S-parameters, the simulation S21 curves show great matching of measured results as **Figure 15(b)**.

4.2 Ge/Si APD receiver's sensitivity and overload performance

Sensitivity and overload performance are two mostly critical system-level specifications for high-speed receivers. For sensitivity, it is typically defined at certain signal-to-noise ratio (SNR). APD receiver's signal-to-noise ratio (SNR) is related to several parameters including APD responsivity, gain and dark current, TIA noise current, and receiver bandwidth like following equation [77]:

$$\frac{S}{N} = \frac{\left(\frac{1}{2}\right)\left(\frac{q\eta P_S}{h\nu}\right)^2}{2q\left(I_{dark} + I_{photo}\right)FB + \frac{<i_{TIA}^2>}{M^2}} \tag{3}$$

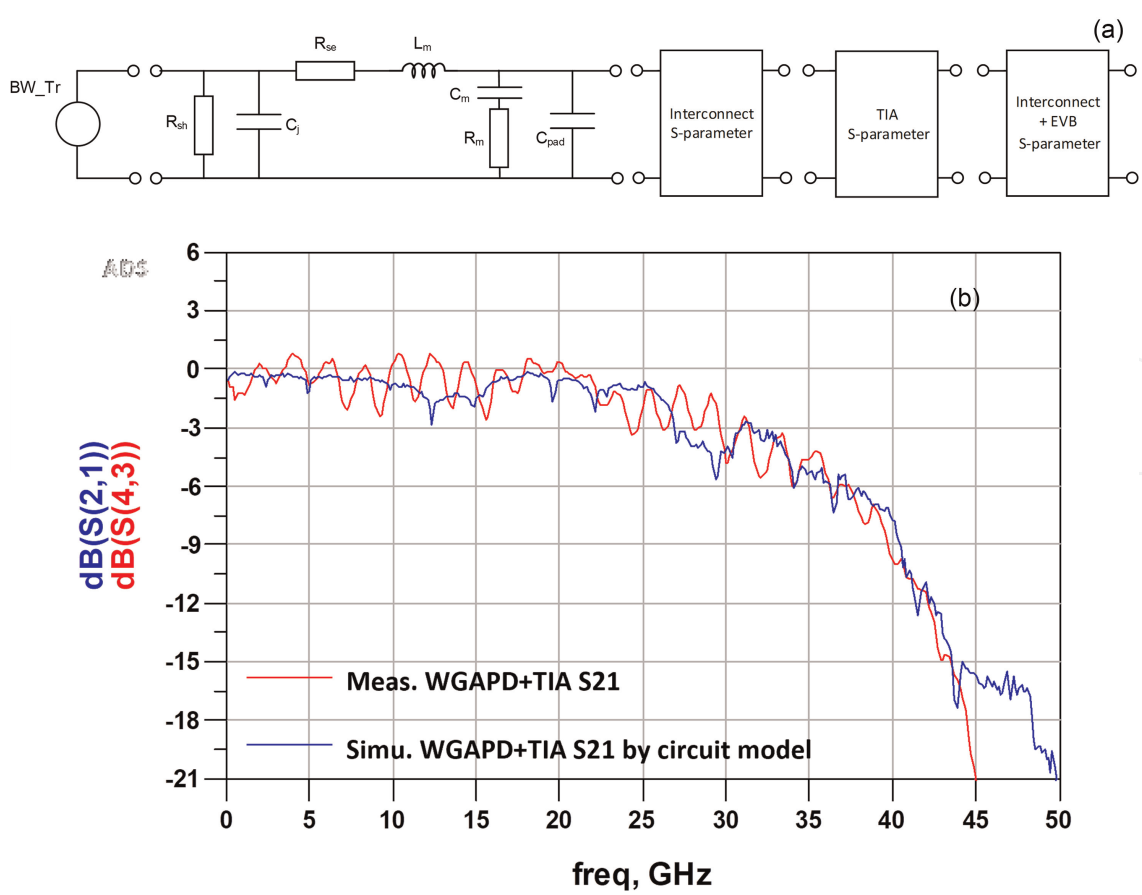

Figure 15.
a) Ge/Si APD receiver model; b) Ge/Si APD receiver measured S21 and fitting results.

Here, F is excess noise factor and related to APD gain (M) and ionization coefficient ratio k:

$$F = kM + \left(2 - \frac{1}{M}\right) \times (1 - k) \tag{4}$$

From Eqs. (3) and (4), TIA noise current is inversely proportional to APD gains, and excess noise factor is increasing with gain. APD SNR presents a parabolic curve with gain increasing as shown in **Figure 16**:

On the other hand, the receiver overload happens at rms photocurrent value larger than the threshold of TIA [79]. And rms photo current is given by [80]:

$$i_p = \frac{q\eta m P_o M}{\sqrt{2}h\nu} \tag{5}$$

For APD operating gain range of 1–8, APD receiver's sensitivity P_s is improved at larger gain, but overload P_o is degraded. Therefore, a trade-off is necessary for balancing sensitivity and overload. **Figure 17** presents our recess-type Ge/Si APD BER results. Our receiver unstressed sensitivity reaches −18.9 dBm at BER 2×10^{-4}, which provide >5 dB margin compared to 100 Gb/s per lane 40 km sensitivity specification (−13.8 dBm) [81]. Moreover, our receiver presents a flat BER below 10^{-7} with input optical power up to 0 dBm that provide enough margins for overload specifications (−2.6 dBm) [81].

As shown in **Figure 17**, Ge/Si WGAPD receiver provides ∼8 dB margin compared to PIN photodiode solution. It provides record ∼19 dB dynamic range for 106 Gb/s operating, which supports both short reach applications like back-to-back and 40 km long-reach applications.

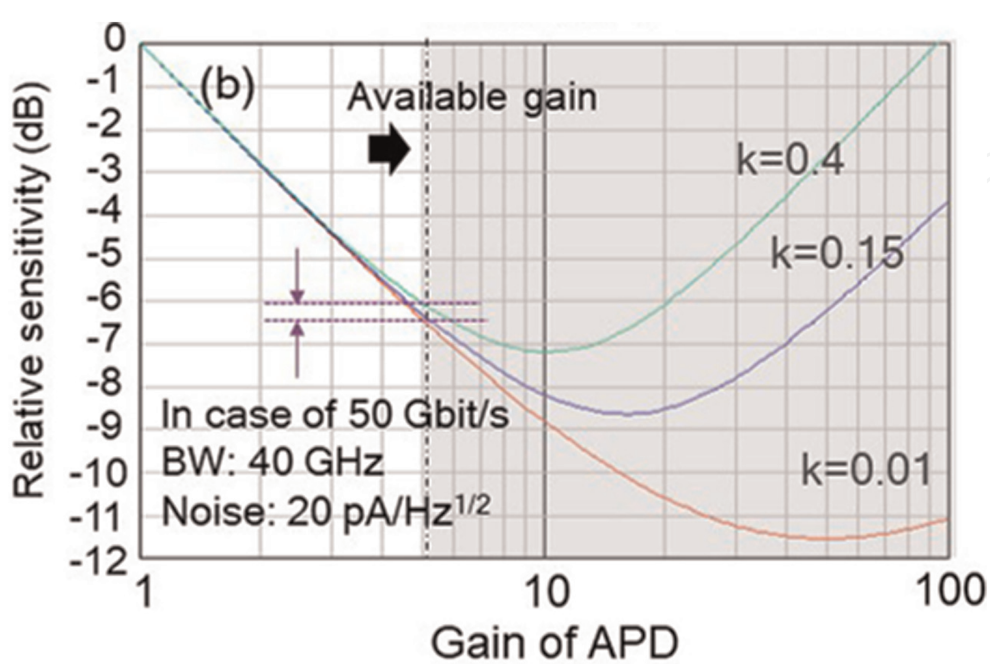

Figure 16.
50 Gb/s APD receiver sensitivity vs. gain [78].

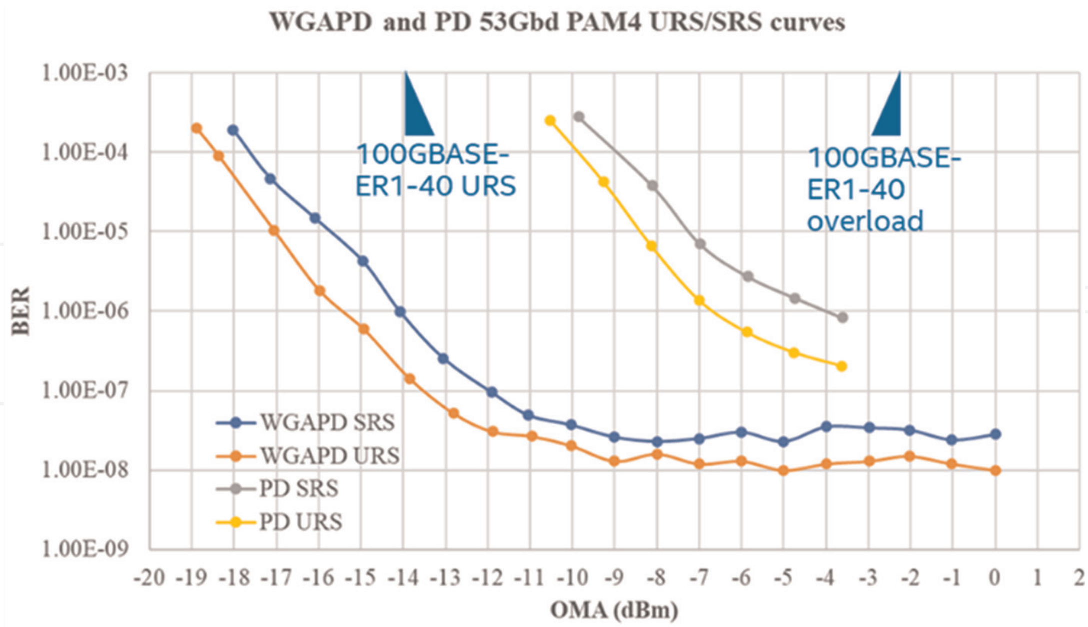

Figure 17.
106 Gb/s WGAPD and PD receiver performance vs. IEEE 100G-ER1-40 specification [2].

4.3 Ge/Si APD receiver's current and future commercial applications

5G mobile network infrastructures are deployed worldwide. The data rate reaches 50 Gb/s at 5G front haul [82] and increases to 100 Gb/s at 5G middle/back hauls [83]. These applications require high-sensitivity devices for achieving passive networks without optical amplifiers. Because of Ge/Si superior sensitivity and overload at 100 Gb/s, millions of Ge/Si APD receivers are deployed in 5G wireless systems in last few years [84]. Moreover, Ge/Si APDs have more important applications including next-generation fiber communication systems. One example is coming 800G/1.6 T inter-connects inside data centers with 200 Gb/s per lane data rate. Such high-bandwidth

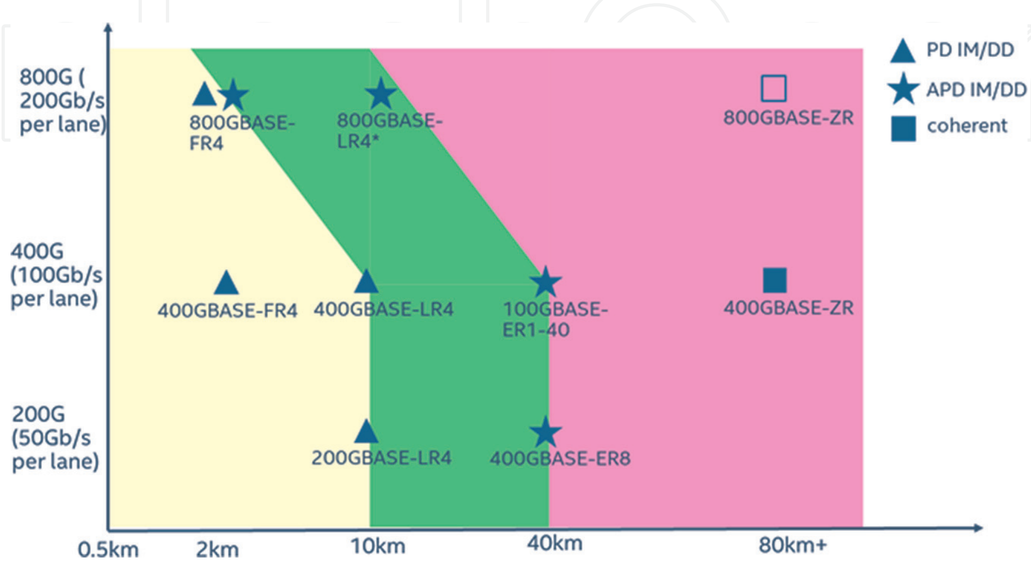

Figure 18.
IEEE/MSA standards and receiver solutions (current and future).

applications degrade receiver's sensitivities, and photodiodes can only cover operation distances within 2 km [85, 86]. For other 2 km and beyond applications, APD receivers become one of most attractive solutions because of their high performance. **Figure 18** presents various IEEE standards and related receivers' solutions with different data rates and operation distances:

5. Conclusion

In this chapter, we study structure evolutions from Ge/Si NIAPD to recess-type Ge/Si WGAPD. The latest structure provides high responsivity and flat operation spectrum suitable for WDM schemes. Moreover, we comprehensively analyze Ge/Si APD's essential characteristics including shallow-level defect states, heterojunction type, NDR effect, and gain-bandwidth products. These studies provide fundamental understandings of Ge on Si materials and related APD's performance. Furthermore, we review our Ge/Si APD receivers' sensitivity and overload including receivers' applications in current and future optical fiber and data communications.

Author details

Mengyuan Huang[1*], Kelly Magruder[2], Yann Malinge[1], Parastou Fakhimi[2], Hao-Hsiang Liao[1], David Kohen[2], Gregory Lovell[1], Wei Qian[1], Kiyoung Lee[2], Carsten Brandt[2], Mahtab Hakami[1], Yen-jung Chen[1], Erin Carabajal[2], Erle Guillermo[2], Seth Slavin[2] and Ansheng Liu[1]

1 Intel Corporation, Santa Clara, CA, USA

2 Intel Corporation, Rio Rancho, NM, USA

*Address all correspondence to: mengyuan.huang@intel.com

References

[1] Huang M et al. Breakthrough of 25Gb/s germanium on silicon avalanche photodiode. In: Optical Fiber Communication Conference, Paper Tu2D.2. 2016

[2] Huang M et al. Recess-type waveguide integrated germanium on silicon avalanche photodiode. In: Optical Fiber Communication Conference, Paper F2C.3. 2021

[3] Campbell JC et al. Recent advances in avalanche photodiodes. In: Optical Fiber Communications Conference and Exhibition (OFC), M3C.1. 2015

[4] Zhang J et al. 64Gb/s PAM4 and 160Gb/s 16QAM modulation reception using a low-voltage Si-Ge waveguide-integrated APD. Optics Express. 2020; **28**(16):23266-23273

[5] Reinsel D et al. The Digitization of the World from Edge to Core, An IDC White Paper. 2018

[6] LightCounting Ethernet Transceivers Forecast. LightCounting, March 2020

[7] Yole: Optical transceiver for Datacom & Telecom, Marketing and Technology Report. 2022

[8] Mobile Optical Pluggables (MOPA), Technical Paper. 2022

[9] Szczerba K et al. 4-PAM for high-speed short-range optical communications. Journal of Optical Communications and Networking. 2012; **4**(11):885-894

[10] Cole C. Ideal SNR penalties, IEEE 802.3 interim meeting, 400Gb/s Ethernet task force. 2014

[11] Yoshimatsu T et al. Compact and high-sensitivity 100-Gb/s (4 × 25 Gb/s) APD-ROSA with a LAN-WDM PLC demultiplexer. Optics Express. 2012;**20**(26):B393-B398

[12] Harstead E et al. From 25 Gb/s to 50 Gb/s TDM PON: Transceiver architectures, their performance, standardization aspects, and cost modeling. Journal of Optical Communications and Networking. 2020; **12**(9):D17-D26

[13] Nakagawa J et al. First Demonstration of 10G-EPON and GE-PON Co-Existing System Employing Dual-Rate Burst-Mode 3R Transceiver, Optical Fiber Communication Conference, paper PDPD10, 2010

[14] Nada M et al. High-sensitivity 25 Gbit/s avalanche photodiode receiver optical sub-assembly for 40 km transmission. Electronics Letters. 2012; **48**(13):777–778

[15] Shiba K et al. Theoretical and experimental study on waveguide avalanche photodiodes with an Undepleted absorption layer for 25-Gb/s operation. Journal of Lightwave Technology. 2011;**29**(2):153–161

[16] Nada M et al. A 42-GHz bandwidth avalanche photodiodes based on III-V compounds for 106-Gbit/s PAM4 applications. Journal of Lightwave Technology. 2019;**37**(2):260-265

[17] Nada M et al. 106-Gbit/s PAM4 40-Km Transmission Using an Avalanche Photodiode with 42-GHz Bandwidth, Optical Fiber Communication Conference, Paper W4D.2. 2018

[18] Campbell JC et al. Recent advances in avalanche photodiodes. IEEE Journal of Selected Topics in Quantum Electronics. 2004;**10**(4):777–787

[19] Kang Y et al. Monolithic germanium/silicon avalanche photodiodes with 340 GHz gain–bandwidth product. Nature Photonics. 2009;**3**:59–63

[20] Kang Y et al. Ge/Si Avalanche Photodiodes for 1.3μm Optical Fiber Links, IEEE International Conference on Group IV Photonics, Paper 2007 FD6. 2007

[21] Levine BF et al. −29dBm Sensitivity, InAlAs APD-Based Receiver for 10Gb/s Long-Haul (LR-2) Applications, Optical Fiber Communication Conference, Paper OFM5. 2005

[22] Kishino K et al. Resonant cavity-enhanced (RCE) photodetector. IEEE Journal of Quantum Electronics. 1991;**27** (8):2025–2034

[23] Ünlü MS et al. A theoretical study of resonant cavity-enhanced photodetectors with Ge and Si active regions. Applied Physics. 1992;**71**(8): 4049-4058

[24] Dosunmu OI et al. Germanium on double-SOI photodetectors for 1550 nm operation. In: Proc. SPIE 5353, Semiconductor Photodetectors. 2004

[25] Huang M et al. 25Gb/s normal incident Ge/Si avalanche photodiode. In: European Conference on Optical Communication (ECOC). Cannes, France: We.2.4.4. 2014

[26] Huang M et al. Development of Si photonics technology: Ge/Si avalanche photodiode for PON applications. In: Optical Fiber Communication Conference. 2014

[27] Huang M et al. Germanium on silicon avalanche photodiode. IEEE Journal of selected Topics of Quantum Electonics. 2018;**24**(2):1-11. (Article ID: 3800911)

[28] Bennett HE et al. Infrared reflectance of Aluminum evaporated in ultra-high vacuum. Journal of the Optical Society of America. 1963;**53**(9): 1089-1095

[29] Ünlü MS, Strite S. Resonant cavity enhanced photonic devices. Journal of Applied Physics. 1995;**78**:2

[30] IEEE 400GBASE-LR4 specification

[31] IEEE 400GBASE-FR4 specification

[32] Huang M et al. 56GHz Waveguide Ge/Si Avalanche Photodiode, Optical Fiber Communication Conference, Paper W4D.6. 2018

[33] Wang X, Liu J. Step-coupler for efficient waveguide coupling to Ge/Si avalanche photodetectors. IEEE Photonics Technology Letters. 2011;**23** (3):146-148

[34] Kang Y et al. High performance Ge/Si avalanche photodiodes development in intel. In: Optical Fiber Communication Conference, Paper OWZ1. 2011

[35] Piels M, Bowers JE. 40 GHz Si/Ge uni-traveling carrier waveguide photodiode. Journal of Lightwave Technology. 2014;**32**(20):3502-3508

[36] Ishikawa Y, Wada K. Near-infrared Ge photodiodes for Si photonics: Operation frequency and an approach for the future. IEEE Photonics Journal. 2010;**2**(3):306-320

[37] Wang G et al. A model of threading dislocation density in strain-relaxed Ge and GaAs epitaxial films on Si (100). Applied Physics Letters. 2009;**94**: 102115-1–102115-3

[38] Kim M, Hashemi P, Hoyt JL. Increased critical thickness for high Ge-

content strained SiGe-on-Si using selective epitaxial growth. Applied Physics Letters. 2010;**97**(26):262106-1–262106-3

[39] Oldham WG, Milnes AG. Interface states in abrupt semiconductor heterojunctions. Solid-State Electronics. 1964;**7**(2):153-165

[40] Claeys C, Simoen E. Germanium-Based Technologies from Materials to Devices. Elsevier; 2007. ISBN: 978-0-08-044953-1

[41] Patel N. Understanding Defects in Germanium and Silicon for Optoelectronic Energy Conversion [MIT Ph.D thesis]. 2016

[42] Giovane L et al. Correlation between leakage current density and threading dislocation density in SiGe p-i-n diodes grown on relaxed graded buffer layers. Applied Physics Letters. 2001;**78**:541-543

[43] Yeh W et al. Sputter epitaxial growth of flat germanium film with low threading-dislocation density on silicon (001). ECS Journal of Solid State Science and Technology. 2014;**3**(10): Q195-Q199

[44] Ohmachi Y et al. The heteroepitaxy of Ge on Si (100) by vacuum evaporation. Journal of Applied Physics. 1983;**54**:5466-5469

[45] Yang R et al. On the frequency dispersion of the capacitance –voltage behavior of epitaxial Ge on Si p+—n junctions. Journal of Applied Physics. 2009;**106**:074511

[46] Madelung O, Rössler U, Schulz M. Semiconductors Group IV Elements, IV-IV and III-V Compounds. Part b - Electronic, Transport, Optical and Other Properties. Springer; 2002

[47] Miller SL. Avalanche breakdown in germanium. Physics Review. 1955;**99**: 1234-1241

[48] Okuto Y, Crowell CR. Threshold energy effect on avalanche breakdown voltage in semiconductor junctions. Solid-State Electronics. 1975;**18**(2): 161-168

[49] Ando H et al. Characteristics of germanium avalanche photodiodes in the wavelength region of 1-1.6μm. IEEE Journal of Quantum Electronics. 1978; **QE-14**(11):804–809

[50] Liu J. Photonics Device. Cambridge University Press; 2005. ISBN: 9780511614255

[51] Kao K et al. Direct and indirect band-to-band Tunneling in germanium-based TFETs. IEEE Transactions on Electron Devices. 2012;**59**(2):292-301

[52] Vossen JL et al. Preparation of surfaces for high quality interface formation. Journal of Vacuum Science and Technology A. 1984;**2**(2):212-215

[53] Nayfeh A. Heteroepitaxial growth of relaxed germanium on silicon [Ph.D thesis]. Stanford University; 2006

[54] Brabant PD et al. Moisture requirements to reduce interfacial sub-oxides and lower hydrogen pre-bake temperatures for RPCVD Si epitaxy. Journal of Crystal Growth. 2013;**381**: 33-36

[55] Raynal P et al. Wet and Siconi® cleaning sequences for SiGe p-type metal oxide semiconductor channels. Microelectronics Engineering. 2018;**187–188**:84-89

[56] Haddara YM et al. Silicon-germanium: Properties, growth and applications. In: Chapter 22 of Springer

Handbook of Electronic and Photonic Materials. 04 October 2017. ISBN 978-3-319-48933-9

[57] Virgilio M, Grosso G. Type-I alignment and direct fundamental gap in SiGe based heterostructures. Journal of Physics: Condensed Matter. 2006;**18**: 1021-1031

[58] Liu J et al. Ge-on-Si optoelectronics. Thin Solid Films. 2012;**520**(8):3354-3360

[59] Teherani J et al. Extraction of large valence-band energy offsets and comparison to theoretical values for strained-Si/strained-Ge type-II heterostructures on relaxed SiGe substrates. Physical Review B. 2012;**85**: 205308

[60] Vines P et al. High performance planar germanium-on-silicon single-photon avalanche diode detectors. Nature Communications. 2019;**10**:1-8. Article number: 1086

[61] Thorburn F et al. Ge-on-Si single-photon avalanche diode detectors for short-wave infrared wavelengths. Journal of Physics: Photonics. 2022;**4**: 012001

[62] Kim G et al. Enhanced frequency response associated with negative photoconductance in an InGaAs/InAlAs avalanche photodetector. Applied Physics Letters. 2003;**83**(6):1249-1251

[63] Moise TS et al. Optically switched resonant tunneling diodes. Applied Physics Letters. 1995;**66**(9):1104-1106

[64] England P et al. Optical switching in a resonant tunneling structure. Applied Physics Letters. 1991;**58**(9):887-889

[65] Lyo I, Avouris P. Negative differential resistance on the atomic scale: Implications for atomic scale devices. Science. 1989;**245**(4924): 1369-1371

[66] Zaoui WS et al. Frequency response and bandwidth enhancement in Ge/Si avalanche photodiodes with over 840GHz gain-bandwidth-product. Optics Express. 2009;**17**(15): 12641-12649

[67] Kim G et al. NDR-effect vertical-illumination-type Ge-on-Si avalanche photodetector. Optics Letters. 2018; **43**(22):5583-5586

[68] Ning D et al. High speed waveguide-integrated Ge/Si avalanche photodetector. In: Optical Fiber Communication Conference, Paper OM3K.3. 2013

[69] Yuan Y et al. 64 Gbps PAM4 Si-Ge waveguide avalanche photodiodes with excellent temperature stability. Journal of Lightwave Technology. Light Counting Ethernet Transceivers Forecast. LightCounting. March 2020; **38**(17):4857-4866

[70] Wang G et al. A time-delay equivalent-circuit model of ultrafast p-i-n photodiodes. IEEE Transactions on Microwave Theory and Techniques. 2003;**51**(4):5583-5586

[71] Dai D et al. Equivalent circuit model of a Ge/Si avalanche photodiode. In: IEEE International Conference on Group IV Photonics. 2009

[72] Novack A et al. Germanium photodetector with 60 GHz bandwidth using inductive gain peaking. Optics Express. 2013;**21**(23):28387-28393

[73] Committee SFF. SFF-8679 specification for QSFP+ 4X. Hardware and Electrical Specification. SNIA SFF TWG technology affiliate. 2018

[74] Lu Z et al. Geiger-mode operation of Ge-on-Si avalanche photodiodes. IEEE Journal of Quantum Electronics. 2011; **47**(5):731-735

[75] Wang B et al. A compact model for Si-Ge avalanche photodiodes. In: IEEE 15th International Conference on Group IV Photonics (GFP). 2018

[76] Qi X. High frequency characterization and modeling of on-chip interconnects and RF IC wire bonds [Ph.D thesis]. Stanford University; 2001

[77] Gao J. Optoelectronic Integrated Circuit Design and Device Modeling. New York, NY, USA: Wiley; 2011

[78] Nada M et al. High-speed III-V based avalanche photodiodes for optical communications—The forefront and expanding applications. Applied Physics Letters. 2020;**116**:140502-1–140502-5

[79] Mazzini M, 'Technical feasibility of 56Gbaud PAM4 optical link budget based on experimental measurements', 400 Gb/s Ethernet Task Force, SMF Ad Hoc Conference Call. 2014

[80] Sze SM, Ng KK. Physics of Semiconductor Devices. 3rd ed 2007. ISBN: 978-0-470-06832-8

[81] IEEE/MSA 100G-ER1-40km specification

[82] Saliou F et al. Optical access network interfaces for 5G and beyond. Journal of Optical Communications and Networking. 2021;**13**(8):D32–D4

[83] Yu R, Pan D. Silicon Photonics Applications for 5G and Data Centers, Optical Fiber Communication Conference, Paper M3A.5. 2021

[84] Yu R, Chang F. Proposed 800G LR4 Baseline with PAM4 IMDD', IEEE P802.3df 200 Gb/s, 400 Gb/s, 800 Gb/s, and 1.6 Tb/s Ethernet Task Force meeting. March 2022

[85] Tian Y et al. 800Gb/s-FR4 specification and interoperability analysis. In: Optical Fiber Communications Conference and Exhibition, Paper W7F6. 2021

[86] Nagarajan R, Lyubomirsky I. Next-Gen Data Center Interconnects: The Race to 800G. COBO Webcast; 2021